NGC 2782: a merger remnant with young stars in its gaseous tidal tail⋆

S. Torres-Flores,[1,2,3]† C. Mendes de Oliveira,[1] D. F. de Mello,[4,5] S. Scarano, Jr[1]
and F. Urrutia-Viscarra[1]

[1]*Departamento de Astronomia, Instituto de Astronomia, Geofísica e Ciências Atmosféricas da USP, Rua do Matão 1226, Cidade Universitária, 05508-090,*
São Paulo, Brazil
[2]*Laboratoire d'Astrophysique de Marseille, OAMP, Université de Provence & CNRS, 38 rue F. Joliot–Curie, 13388 Marseille, Cedex 13, France*
[3]*Departamento de Física, Universidad de La Serena, Av. Cisternas 1200 Norte, La Serena, Chile*
[4]*Observational Cosmology Laboratory, Code 665, Goddard Space Flight Center, Greenbelt, MD 20771, USA*
[5]*Catholic University of America, Washington, DC 20064, USA*

ABSTRACT

We have searched for young star-forming regions around the merger remnant NGC 2782. By using *Galaxy Evolution Explorer* far-ultraviolet and near-ultraviolet imaging and H I data we found seven ultraviolet sources, located at distances greater than 26 kpc from the centre of NGC 2782, and coinciding with its western H I tidal tail. These regions were resolved in several smaller systems when Gemini/Gemini multi-object spectrograph (GMOS) *r*-band images were used. We compared the observed colours to stellar population synthesis models and found that these objects have ages of ∼1 to 11 Myr and masses ranging from $10^{3.9}$ to $10^{4.6}$ M$_\odot$. By using Gemini/GMOS spectroscopic data we confirm memberships and derive high metallicities for three of the young regions in the tail ($12+\log(O/H) = 8.74 \pm 0.20$, 8.81 ± 0.20 and 8.78 ± 0.20). These metallicities are similar to the value presented by the nuclear region of NGC 2782 and also similar to the value presented for an object located close to the main body of NGC 2782. The high metallicities measured for the star-forming regions in the gaseous tidal tail of NGC 2782 could be explained if they were formed out of highly enriched gas which was once expelled from the centre of the merging galaxies when the system collided. An additional possibility is that the tail has been a nursery of a few generations of young stellar systems which ultimately polluted this medium with metals, further enriching the already pre-enriched gas ejected to the tail when the galaxies collided.

Key words: galaxies: interactions – intergalactic medium – galaxies: star clusters: general.

1 INTRODUCTION

The intergalactic medium (IGM) of interacting galaxies and the tidal tails of mergers have shown to commonly be the birthplace of a number of new stellar systems. These systems span the range from small clusters (Knierman et al. 2003; Tran et al. 2003) and intergalactic H II regions (IH II; e.g. Mendes de Oliveira et al. 2004)

to tidal dwarf galaxies (TDGs; Mirabel, Dottori & Lutz 1992; Duc & Mirabel 1998; Weilbacher et al. 2000; Weilbacher, Duc & Fritze-v. Alvensleben 2003; Bournaud et al. 2004; Mundell et al. 2004; Mendes de Oliveira et al. 2006).

Since the total luminosity of these young stellar systems is mostly dominated by the ultraviolet (UV) ionizing radiation coming from massive stars, the use of the *Galaxy Evolution Explorer* (*GALEX*) satellite (Martin et al. 2005) has become an important tool to study the star formation processes and the stellar populations of these systems (Neff et al. 2005; Hancock et al. 2007, 2009; de Mello, Torres-Flores & Mendes de Oliveira 2008a; Smith et al. 2008, 2010; Boquien et al. 2009, 2010; Torres-Flores et al. 2009).

Another crucial ingredient for the study of the stellar populations and formation processes of young stellar systems is the knowledge of their element abundances. This can, in fact, constrain the formation scenario of these stellar associations. For example, Weilbacher et al. (2003) studied the oxygen abundance of several knots in tidal features which had been classified as TDG candidates.

These authors found metallicities similar to the values found in the outer disc of the spirals from which these knots were formed, which suggests that these objects were born from a pre-enriched material. In a lower mass regime, Mendes de Oliveira et al. (2004) studied spectroscopically four H II regions in the IGM of the compact group HCG 92. These authors found high metallicities for these regions, also suggesting that they were formed from a pre-enriched material.

In this context, we have searched for star-forming regions in the merger remnant NGC 2782, which include spectroscopic confirmation for three of the sources. This allows us to study the formation of stellar clusters and the enrichment of the IGM, and to attempt to identify the evolutionary stage of the merger.

NGC 2782 (Arp 215) is at a distance of 34 Mpc (Smith 1994). Its heliocentric radial velocity is $2543 \pm 2 \, \text{km s}^{-1}$ [from NASA/IPAC Extragalactic Database (NED)]. This galaxy shows a prominent tidal tail detected in H I, located to the western side of the object. A second tidal tail formed by a stellar component is seen to the east side of the galaxy. Smith (1994) reports the presence of arcs and ripples in this system. These kinds of signatures are common in colliding and merging galaxies (Schweizer 1980, 1982). Due to all the features listed above, Smith (1994) and Smith et al. (1999) classified this system as a merger remnant. In the tidal tail located to the east side of the galaxy, Yoshida et al. (1994) detected a dwarf galaxy in formation and molecular gas was found by Smith et al. (1999) in this region. No molecular gas was found in the western tidal tail (Smith et al. 1999; Braine et al. 2001). New CO observations of the central region of NGC 2782 are shown in Hunt et al. (2008). In a search for extended UV discs, Thilker et al. (2007) included the merger remnant NGC 2782 in its sample. These authors report the presence of UV clumps in the north-west tidal tail of NGC 2782, suggesting that star formation is taking place in this tail.

Recently, Werk et al. (2011) studied the oxygen abundances of several outlying H II regions in a sample of local galaxies, where NGC 2782 was included. Theses authors concluded that most of their systems have flat metallicity gradients. In Section 4.2 we discuss the results found by Werk et al. with ours.

This paper is organized as follows. In Sections 2 and 3 we present the data and data analysis. In Section 4 we present the results. In Section 5 we discuss our results and in Section 6 we present our main conclusions.

2 DATA

2.1 Ultraviolet data

The UV *GALEX* images of NGC 2782 have been published by Thilker et al. (2007). In our case, the UV data analysed in this work were taken from the public archival data of the *GALEX* satellite. From this archive, we used images in the near-ultraviolet (NUV, $\lambda_{\text{eff}} = 2271$ Å) and far-ultraviolet (FUV, $\lambda_{\text{eff}} = 1528$ Å) bands. In the NUV band, the exposure time was 2109 s, and in the FUV band, it was 2108 s. FUV and NUV fluxes were calculated using Morrissey et al. (2005) $m_\lambda = -2.5 \log [F_\lambda / a_\lambda] + b_\lambda$, where $a_{\text{FUV}} = 1.4 \times 10^{-15} \, \text{erg s}^{-1} \, \text{cm}^{-2} \, \text{Å}^{-1}$, $a_{\text{NUV}} = 2.06 \times 10^{-16} \, \text{erg s}^{-1} \, \text{cm}^{-2} \, \text{Å}^{-1}$, $b_{\text{FUV}} = 18.82$ and $b_{\text{NUV}} = 20.08$ for FUV and NUV, respectively. The fluxes were multiplied by the effective filter bandpass ($\Delta \lambda_{\text{FUV}} = 269$ Å and $\Delta \lambda_{\text{NUV}} = 616$ Å) to give units of erg s^{-1} cm^{-2}. The *GALEX* fields of view are 1°28 and 1°24 in FUV and NUV, respectively, and the pixel scale is 1.5 arcsec pixel^{-1}. The images had a resolution (full width at half-maximum) of 4.2 and 5.3 arcsec in FUV and NUV, respectively.

2.2 *r*-band and spectroscopic data

Observations of NGC 2782 were carried out with the Gemini multi-object spectrograph (GMOS) at the Gemini north observatory as part of the science programme GN-2009B-Q-113. *r*-band images for two fields in NGC 2782 were observed. Fields were centred on the western gaseous tidal tail (RA = 09^{h}13^{m}53^{s}5, Dec. = 40°09′31″6, J2000) and on the object NGC 2782 (RA = 09^{h}14^{m}03^{s}2, Dec. = 40°06′59″1, J2000). The exposure times for both *r*-band images were 15 min, under a seeing of 0.54 and 0.77 arcsec, respectively. Zero-point calibrations were taken from the Gemini website. We checked these values using a few bright stars (on the same field) from the Sloan Digital Sky Survey (SDSS) data base (Abazajian et al. 2009).

Archival GMOS multislit spectroscopic exposures (3 × 1200 s) were available for five objects on the western tidal tail of NGC 2782, covering from 3400 to 6100 Å (grating B600). These Gemini data were originally acquired by Werk et al. (2011), who provide more details on the observations and an independent reduction and analysis (science programme GN-2008A-Q-31). In this work, these spectra were reduced using standard routines in IRAF.[1] In addition, an SDSS spectrum (covering from 3800 to 9229 Å) was available for one object in the star-forming arc along the inner ripple of NGC 2782. This object, whose coordinates are RA = 09^{h}14^{m}02^{s}6 and Dec. = +40° 06′ 47″2 (J2000), was already detected in the Hα images shown by Hodge & Kennicutt (1983), Smith (1994, fig. 6) and Jogee, Kenney & Smith (1998, fig. 4).

2.3 Neutral gas

The calibrated H I data of NGC 2782 were taken from the NED. This has a spectral resolution of 31.5 km s^{-1}. Details about the observation can be found in Smith (1994).

3 DATA ANALYSIS

3.1 Selection criteria

In this work, we are interested in searching for young star-forming regions in the gaseous tidal tail of NGC 2782; therefore, no regions on the main body of this galaxy were taken into account. The spectrum of a typical star-forming region is obviously characterized by a strong Hα line. If we simulate an instantaneous burst of star formation using the STARBURST99 model (SB99; Leitherer et al. 1999), the lifetime of the Hα line, given a fixed mass of $10^6 \, \text{M}_\odot$, is of the order of 10 Myr (for a solar metallicity). This is basically produced by the short lifetime of massive stars (OB stars). When this age is linked to the UV colours, it results in a colour FUV–NUV = −0.10. However, when the metallicity increases (to $Z = 2.5 \, \text{Z}_\odot$, for instance) the models predict an age of 10 Myr for a colour FUV–NUV = 0.03. In this theoretical scenario, objects having colours bluer than FUV–NUV∼0 have experienced a recent episode of star formation.

On the other hand, we note what has been measured from observations. The colours FUV–NUV of the objects studied in Mendes de Oliveira et al. (2004), as measured in Torres-Flores et al. (2009), are (in three of the four regions) FUV–NUV ≤ 0. Also, the TDG candidates studied in de Mello et al. (2008a) with confirmed spectroscopy

---

[1] IRAF is distributed by the National Optical Astronomy Observatories, which are operated by the Association of Universities for Research in Astronomy, Inc., under cooperative agreement with the National Science Foundation. See http://iraf.noao.edu

(de Mello et al. 2012) have colours FUV–NUV ≤ 0. Similar colours were found in the study of Neff et al. (2005) for the star-forming regions detected in four systems with tidal tails. They found three candidates having masses similar to those of confirmed TDGs and colours FUV–NUV of -0.32 ± 0.40, -0.09 ± 0.21 and 0.10 ± 0.23. Therefore, we selected in this study only objects that have FUV–NUV ≤ 0.15 and that are placed within the H I distribution.

3.2 Source extraction and photometry

We detected UV sources using the software SEXTRACTOR (SE; Bertin & Arnouts 1996) over the NUV and FUV images. Due to the large format of the *GALEX* images, star-forming regions were searched for across the whole H I tail. We set the parameter DETECT_THRESH to 1.5σ over the background in the NUV image. We chose 1.5σ since larger σ would cause blending with other sources when using SE automatic apertures. At the end, we had a catalogue with RA and Dec. of each object in the FUV and NUV bands. With this information in hand, we matched the FUV and NUV catalogues using a 3 arcsec radius in order to generate a catalogue in which the sources were identified in both UV bands. As we are interested only in young star-forming regions, we note that our sample as a whole is not complete in FUV magnitudes. FUV and NUV magnitudes were estimated inside a fixed aperture of 4 arcsec radius, centred on the centroid of the light distribution of each NUV band detection, using the task PHOT in IRAF. In this case, the sky subtraction was done by using a sky annulus, where the parameters ANNULUS and DANNULUS were set to 10 pixels and the sky fitting algorithm was the mode of the values inside the annulus. Fixed FUV and NUV magnitudes were corrected by aperture effects by using the task MKAPFILE in IRAF. In order to do that, we used the catalogue of all the sources available in our field, which is provided by the *GALEX* pipeline. In that catalogue, we searched for star-like objects with magnitudes between $15 <$ NUV, FUV < 18 (i.e. non-saturated objects). We used a minimum aperture of 4 arcsec and a maximum one of 60 arcsec. This gives us a correction of FUV $= -0.36 \pm 0.02$ and NUV $= -0.48 \pm 0.03$. In the case of the *r*-band image, the aperture correction was $r = -0.03 \pm 0.01$. Due to its small value (similar to the error determination in the *r*-band magnitudes) we do not take the latter correction into account. Magnitudes were corrected for galactic extinction, using $A_{FUV} = E(B-V) \times 8.29$ and $A_{NUV} = E(B-V) \times 8.18$ (Seibert et al. 2005). We note that due to the *GALEX* spatial resolution, we cannot resolve all of our UV detected regions. In most cases, one UV source will most probably be associated with more than one H II region. The optical *r*-band image will help disentangling the multiple sources. Once the UV-emitting sources were identified, we used the *r*-band image to obtain the magnitudes. For *r*-band magnitudes, we used a fixed aperture of 4 arcsec radius centred on the UV *GALEX* emission. *r*-band magnitudes were corrected by Galactic extinction using the Savage & Mathis (1979) extinction law and $E(B-V)$ given by Schelegel, Finkbeiner & Davis (1998).

3.3 Ages and masses: photometric estimates

For each region, ages were estimated from the FUV–NUV and FUV–*r* observed colours and the models given by SB99. For these models, which were tuned for the *GALEX* and *r*-band filters, we used an instantaneous burst, a Salpeter initial mass function (IMF; 0.1–100 M$_\odot$) and a solar metallicity. Models were generated from 1 Myr to 1 Gyr. It is important to note that for low-mass stellar associations, the observed broad-band colours can be affected by an incomplete sampling of the IMF (effect that is not taken into account by the SB99 models, which assume a fully sampled IMF). This fact could produce uncertainties in the dating of low-mass systems (see Cerviño et al. 2003; Cerviño & Valls-Gabaud 2003; Hancock et al. 2008; Popescu & Hanson 2010; da Silva, Fumagalli & Krumholz 2012). In order to know the colour excess ($E(B-V)$) of each star-forming region, two extinction laws have been applied on the theoretical colours, the starburst law given by Calzetti, Kinney & Storchi-Bergmann (1994) and a Milky Way (MW) extinction law, where the A_{FUV} and A_{NUV} values were taken from Seibert et al. (2005) (8.29 and 8.18, respectively) and $A_r = 2.74$ was taken from Savage & Mathis (1979).

One of the main problems in the study of star formation in young clusters is the uncertainty in the value of the internal dust correction. Since there are no infrared data for the clusters, we have estimated ages and extinctions simultaneously by fitting the observed FUV–NUV and FUV–*r* colours to the theoretical ones through a χ^2 minimization calculation. Errors on ages were estimated at a confidence level of 68 per cent, in a similar way as presented by Smith et al. (2008). We note that the ages and $E(B-V)$ used throughout this paper correspond to the values that minimized the χ^2 independent if a starburst or MW extinction law was assumed. Errors on $E(B-V)$ are of the order of 0.3 mag.

We have followed the method used in de Mello et al. (2008a) to estimate the mass of our candidates. Basically, we used the ages and the FUV luminosities of each region to estimate the stellar masses with SB99. The stellar masses were obtained from SB99's monochromatic luminosity, L_{1530}, for an instantaneous burst, Salpeter IMF (from 0.1 to 100 M$_\odot$) and solar metallicity. Since all our candidates present young ages, we note that the luminosities in L_{1530} are dominated by the contribution of massive stars.

3.4 Spectroscopic ages and metallicities

In the SDSS data base we located a calibrated spectrum for one compact object in an arc along a ripple close to the main body of NGC 2782. Due to its large spectral coverage (from 3800 to 9220 Å) we can correct this spectrum for reddening using the Balmer emission lines. The value for the intrinsic Hα/Hβ ratio was taken from Brocklehurst (1971) for $T_e = 10\,000$ K and $N_e = 100$. The spectrum was then corrected using a $c_{H\beta} = 0.85$, using the Cardelli, Clayton & Mathis (1989) MW extinction law.

Gemini/GMOS archival spectroscopic data were available for five objects in the gaseous tidal tail of NGC 2782 (data recently used by Werk et al. 2011), three of which coincided with some of the regions measured by us in this study (regions 5, 6 and 7; see Section 4). We used the task EMSAO of the package RVSAO in IRAF to estimate the radial velocity of the objects. Galactic extinction was calculated using the model by Amôres & Lépine (2005), resulting in an $E(B-V) = 0.08$. The intrinsic reddening of each region was assumed to be that derived in Section 3.3 (see Table 1), given the large uncertainties in the flux estimation of the Hγ line. Galactic and intrinsic corrections were performed using the IDL code FM_UNRED by Fitzpatrick (1999).

We estimated the equivalent width of the Hβ line for the three regions with Gemini/GMOS spectroscopic data. Using the observed and synthetic EW(Hβ) derived from SB99, we estimated the age of each region, assuming a single stellar population. We also measured the [O II] λ3726 Å, [O III] λ4959 Å and [O III] λ5007 Å line fluxes relative to the Hβ line. Using these values we estimated the oxygen abundance using the R_{23} method defined by Edmunds & Pagel (1984, as shown in fig. 2 of Torres-Peimbert, Peimbert &

Table 1. Observed and derived properties for the UV detected regions.

System	RA 2000	Dec. 2000	r^a (mag)	FUV^b (mag)	$FUV-r^c$ (mag)	$FUV-NUV^d$ (mag)	$E(B-V)^e$ (mag)	Age^f (Myr)	$\log M_\star$ (M$_\odot$)	$Distance^g$ (kpc)
1	09:13:48	40:09:56	22.87 ± 0.04	22.47 ± 0.16	-0.39 ± 0.17	-0.26 ± 0.24	0.18/0.23	$1\pm^4_1$	3.9	45
2	09:13:49	40:07:41	>23	22.76 ± 0.18	–	-0.12 ± 0.28	–/0.23	–	–	31
3	09:13:50	40:10:20	22.50 ± 0.03	22.42 ± 0.16	-0.08 ± 0.16	-0.08 ± 0.21	0.16/0.16	$5\pm^6_3$	4.2	46
4	09:13:51	40:08:39	21.27 ± 0.01	22.54 ± 0.17	1.28 ± 0.17	-0.06 ± 0.23	0.26/0.11	$11\pm^{28}_6$	4.6	33
5	09:13:51	40:08:18	22.43 ± 0.03	22.21 ± 0.15	-0.22 ± 0.15	-0.28 ± 0.22	0.22/0.21	$2\pm^4_1$ ($\sim$4)	3.9	31
6	09:13:51	40:08:08	21.44 ± 0.01	21.99 ± 0.13	0.56 ± 0.13	-0.14 ± 0.18	0.34/0.15	$3\pm^4_3$ ($\sim$3)	4.0	30
7	09:13:52	40:07:47	22.23 ± 0.03	22.57 ± 0.18	0.34 ± 0.18	0.14 ± 0.24	0.26/0.20	$6\pm^{23}_6$ ($\sim$2)	4.2	26

^{a}r-band magnitude inside a fixed aperture of 4 arcsec radius and corrected by MW extinction. Region 2 appears to have diffuse emission in the r-band image.
^{b}Fixed FUV-band magnitudes corrected by apertures (as described in Section 3.2) and MW extinction.
^{c}FUV–r colours.
^{d}Magnitudes were measured in a fixed aperture of 4 arcsec radius and corrected by MW extinction. FUV and NUV magnitudes were corrected by aperture, as described in Section 3.2.
^{e}Left values: $E(B-V)$ estimated as in Section 3.3. Right values: $E(B-V)$ estimated by using the H I data of NGC 2782. Total extinction is the sum of the internal and Galactic extinctions (0.13 mag in this band).
^{f}Ages estimated from FUV–NUV and FUV–r. In parenthesis we show the ages estimated from the Hβ equivaland SB99 models.
^{g}Distance from the centre of the galaxy, assuming a position angle and inclination of 0°.

Table 2. Line intensities and oxygen abundances.

ID	$[O II]^a$ 3727	$[O III]$ 4959	$[O III]$ 5007	Hα 6563	$[N II]$ 6584	$EW_{H\beta}$ (Å)	$E(B-V)$	$12+\log(O/H)^b$	$12+\log(O/H)^c$	$12+\log(O/H)^d$
5	4.29 ± 0.14	0.24 ± 0.09	0.65 ± 0.09	–	–	77	0.26^e	8.22 ± 0.20	8.56 ± 0.31	8.74 ± 0.20
6	3.67 ± 0.21	0.17 ± 0.04	0.59 ± 0.04	–	–	192	0.22^e	8.31 ± 0.20	8.65 ± 0.31	8.81 ± 0.20
7	3.75 ± 1.07	0.34 ± 0.08	0.73 ± 0.09	–	–	286	0.34^e	8.30 ± 0.20	8.60 ± 0.31	8.78 ± 0.20
MB	–	0.28 ± 0.01	0.73 ± 0.02	2.01 ± 0.05	0.57 ± 0.01	33	0.85	–	–	8.72 ± 0.10

^{a}Line intensities relative to Hβ.
^{b}Following Pilyugin (2001).
^{c}Following Edmunds & Pagel (1984). We have also used the method given in McCall, Rybski & Shields (1985) and Dopita & Evans (1986), also finding similarly high values for the oxygen abundance.
^{d}Following McGaugh (1991) and using a ionization parameter $U = 0.001$ and $M_u = 60$ M$_\odot$. For the region with the SDSS spectrum (called MB in this table), this value was estimated using Denicoló et al. (2002).
^{e}See Section 3.4.

Fierro 1989). Although R_{23} is a well-studied calibrator that depends on the fine-tuning between oxygen abundance and electron temperature, it has the disadvantage that it is double valued, presenting an upper and lower branch, i.e. for a given value of R_{23}, there are two values for the metallicity (see fig. 9 in McGaugh 1991). This can be explained because at low metallicities, the cooling of the H II region is dominated by collisionally excited Lyman α emission. While the metallicity increases, the contribution of oxygen to cooling is higher. Optical forbidden lines are very important at values of $12+\log(O/H) \sim 8.4$. Beyond that, infrared fine-structure lines dominate the cooling (McGaugh 1991). One way to solve the double-valued problem would be by using the ratio between [N II] and [O II]; however, for none of the regions in the tail we have spectra with enough dynamic range to see these two lines. Further discussion on this point is given in Section 4.2.

We also estimated the oxygen abundance using the results found by Pilyugin (2001), who used an empirical approach, which is optimized for high-metallicity H II regions. In spite of the method shown by Pilyugin (2001) being optimized for high-metallicity H II regions, van Zee & Haynes (2006) found that when this method is compared with direct abundances calculations, the residuals of that comparison seem to be correlated with the ionization parameter of the H II regions. van Zee & Haynes (2006) found that this systematic trend does not exist in the case of the semi-empirical method shown in McGaugh (1991). For this reason, we have also used this

latter method to estimate the oxygen abundance of the star-forming regions to compare the results with the other methods mentioned above.

In the case of the SDSS spectrum, which does not have the [O II] line, we estimated the oxygen abundance by using the N2 method (Denicoló, Terlevich & Terlevich 2002).

4 RESULTS

In the following we list the main results derived from the photometry and spectroscopy for the star-forming regions detected in NGC 2782. Photometric results are summarized in Table 1, while spectroscopic results are listed in Table 2.

4.1 Main photometric properties of the star-forming regions

We found seven blue UV-emitting regions in the western tidal tail of NGC 2782. In Fig. 1 we show the NUV and r-band images of the gaseous tidal tail of NGC 2782. We also show a close-up of each region. In Fig. 2 we show an r-band image (taken with Gemini/GMOS) of the main body of NGC 2782. Five of the seven detected regions are enclosed by a white circle (the other two regions are off the field of view). As already mentioned, we located the SDSS spectrum of a compact region close to the centre of NGC 2782. In Fig. 2 we show a zoom of such an object.
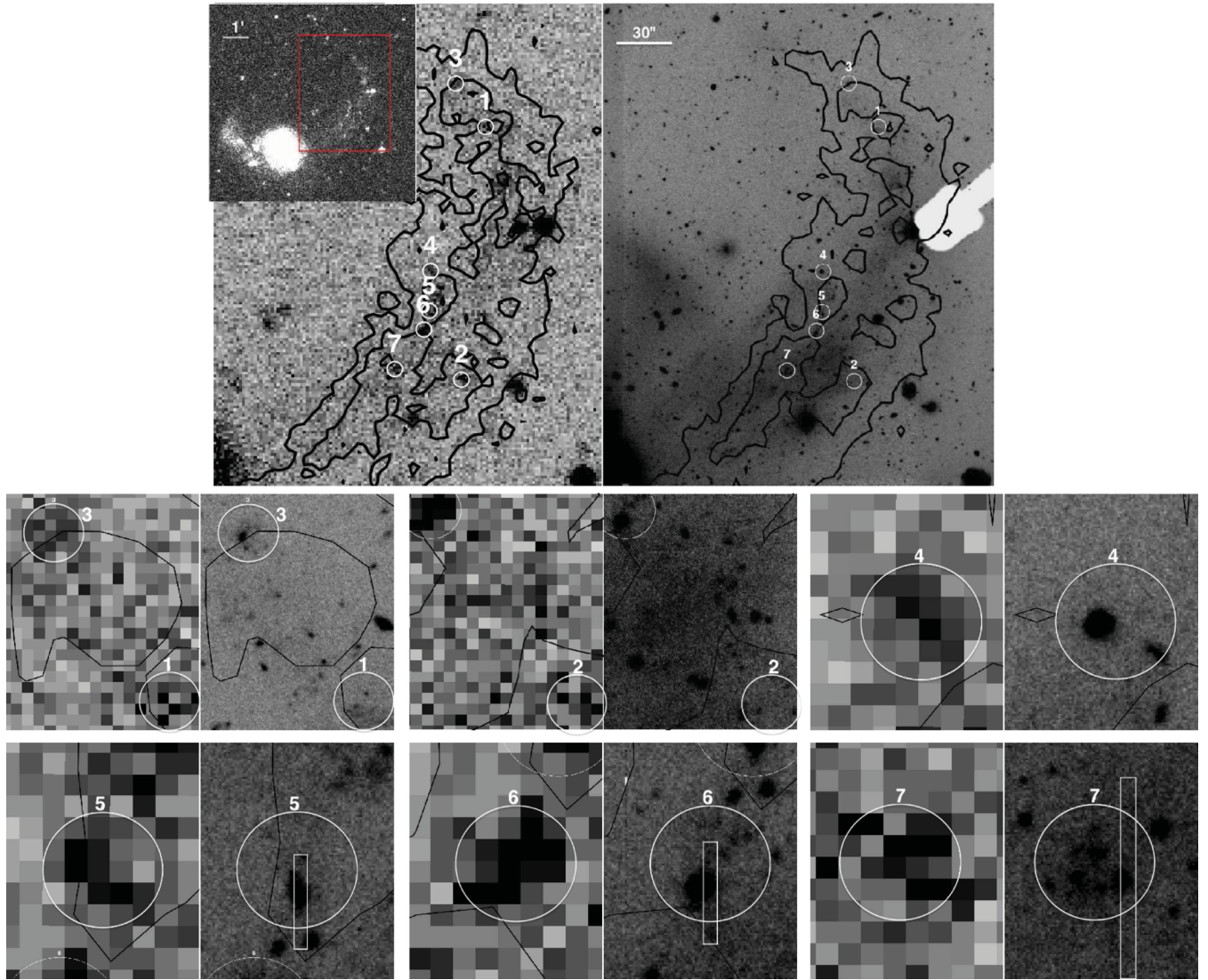
Figure 1. Top-left: NUV-band image of the H I tidal tail of NGC 2782. An NUV-band image of the entire target is shown in the upper-left corner. Top-right: *r*-band image of the tail. The numbered circles (4 arcsec radius) show the detected regions. The contours represent the H I distribution taken from Smith (1994). Bottom images: close-up of the detected regions (left-hand side: NUV-band image; right-hand side: *r*-band image). The Gemini *r*-band image resolved the UV detections in several smaller stellar clusters, as exemplified in the lowest six panels. The white rectangles over regions 5, 6 and 7 indicate, approximately, the position of the slit in the spectroscopic observation.

In Fig. 2 we show the *r*-band image of the main body of NGC 2782. This system clearly shows shells. From this figure, we note that in the region where the UV-emitting sources were found, there is diffuse emission, probably associated with an old stellar population. Diffuse emission is also present in the south and south-east regions of NGC 2782.

In Fig. 3 we plot the FUV–NUV versus FUV–*r* colours for the regions located in the gaseous tidal tail of NGC 2782 (black stars). In the same plot, we include the SB99 models in the cases of no extinction (black line), MW (blue line) and starburst (red line) extinction laws. Best parameters (ages and respective uncertainties and extinctions) are listed in Table 1. We found ages ranging from ∼1 to 11 Myr. Regions numbered 1, 5 and 6 are the youngest objects found in the gaseous tidal tail of NGC 2782. Interestingly, regions 5 and 6 are detected in the Hα image of the system (de Mello et al. 2012).

As described in Section 3.3, we have calculated the colour excess ($E(B - V)$) of the star-forming regions of NGC 2782. Regions 4, 6 and 7 have the highest colour excess of this sample, with values of $E(B - V) = 0.26$, 0.34 and 0.26, respectively. On the other hand, region 3 has the lowest reddening of 0.16 mag. In order to check these values, we have computed the colour excess for each region by using the H I map of NGC 2782 (Smith 1994). In order to do that, we used equation C1 in Minchin et al. (2003) to estimate the H I column density and we assume the standard Galactic N(H)-to-extinction ratio of $N(H)/E(B - V) = 5.8 \times 10^{21}$ atoms cm^{-2} mag^{-1} (Bohlin, Savage & Drake 1978). In Table 1 we listed the values of $E(B - V)$ derived from neutral hydrogen. Within the uncertainties, the $E(B - V)$ values from the two methods are reasonably consistent.

The mass estimates for the six star-forming objects (with photometrically derived ages) span a range of $3.9 < \log M_{\odot} < 4.6$ (Table 1), which are similar to the masses inferred for the
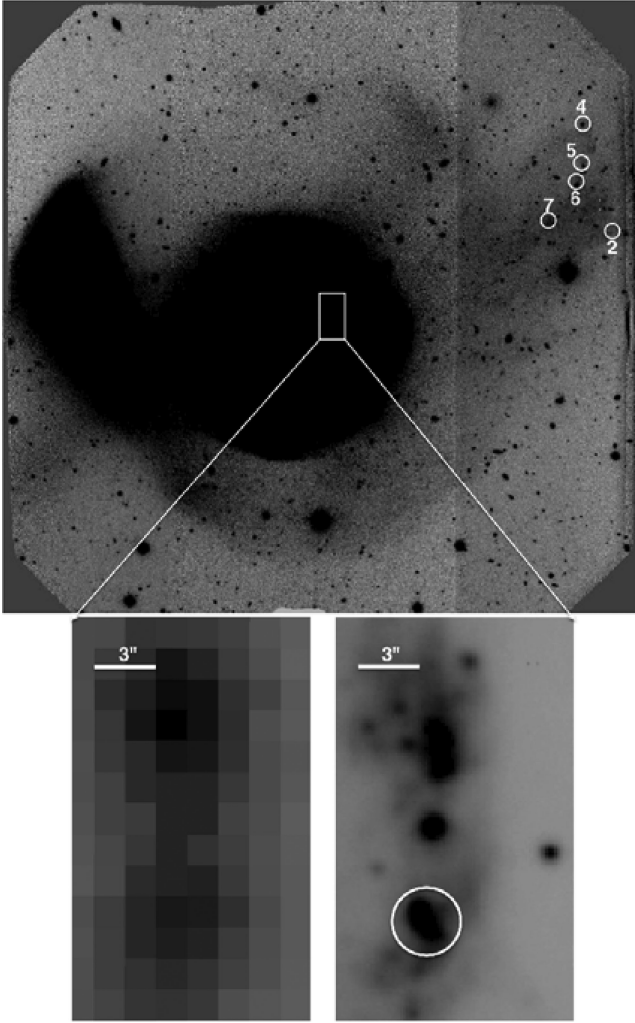
Figure 2. *r*-band image of NGC 2782. UV-detected star-forming regions are marked with a white circle of 4 arcsec radius. Shells structures can be seen around the main body of NGC 2782. The white square in the main body of NGC 2782 shows the location of the compact object with the SDSS spectrum. We also show a close-up of this object in the NUV and *r*-band filters (left- and right-hand images, respectively). The source is indicated by a white circle (RA = 09^h 14^m 02$.\!\!^s$6, Dec. = +40°06′47″.2).

intergalactic H II regions detected in Mendes de Oliveira et al. (2004), for which the mean mass is log($M_\odot$) = 4.5. The masses of the star-forming regions in NGC 2782 are slightly lower than the masses of the regions found in the tail of Arp 285 (Smith et al. 2008), which range from 4.3 < log$M_\odot$ < 5.9. In the same context, a few of the sources in the tail of Arp 82 (Hancock et al. 2007) have larger masses than those in NGC 2782, reaching masses of log($M_\odot$) = 7.9, in a similar way to the southern source located in the tail of Arp 105, which has a mass of log($M_\odot$) = 7.8 (Boquien et al. 2010). None of the regions detected in this work have masses typical of TDGs which are usually defined to have masses larger than log($M_\odot$) ∼ 8.11 (Duc & Mirabel 1998).

We estimated the distance from the centre of NGC 2782 to each individual region (Table 1). The closest object is located at 26 kpc from the centre of the galaxy, having an age of 6 Myr. If this object was thrown out of the disc of the main galaxy in some galaxy–galaxy interaction, it should have been expelled with an unlikely high velocity of ∼4200 km s^{-1} (assuming a constant velocity, i.e.
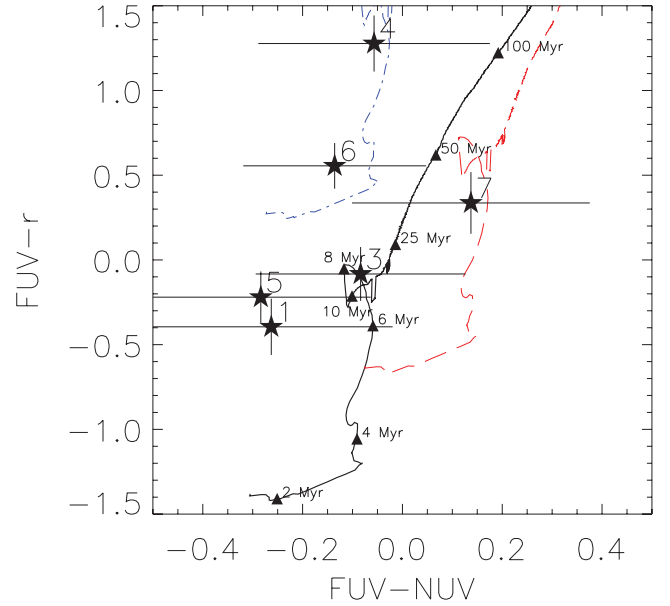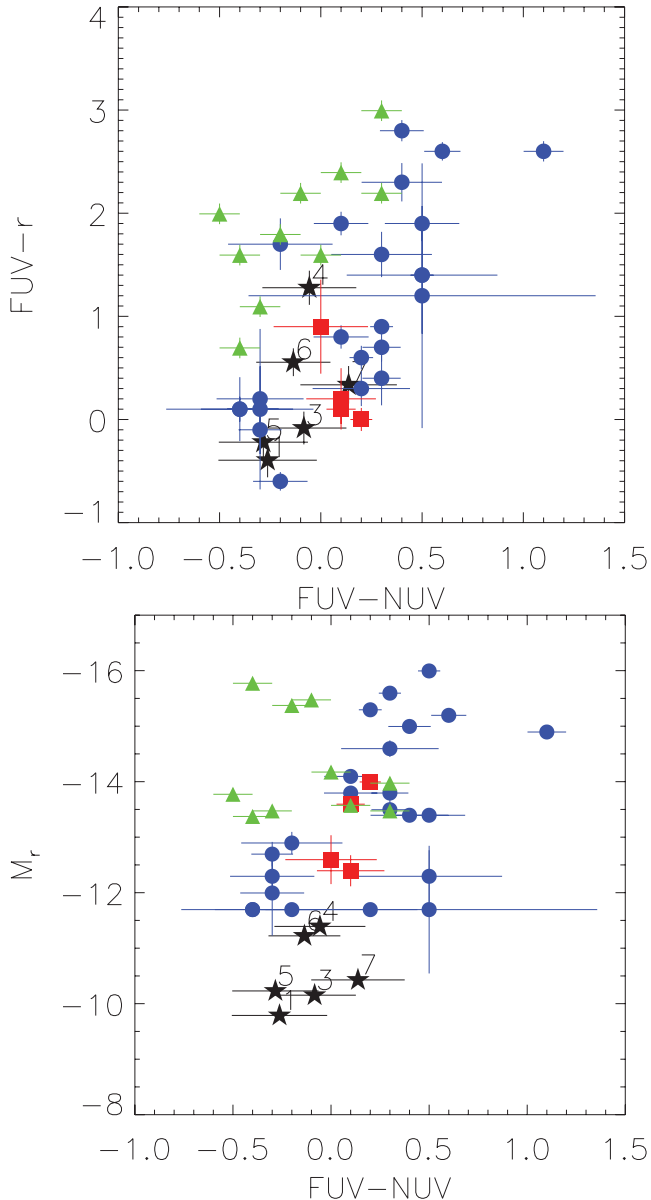

Figure 3. *GALEX* FUV–NUV versus FUV–*r* of the star-forming regions (black stars). Models from SB99 are shown as a solid black line (no extinction correction), dash–dotted blue line (MW extinction law with an *E(B − V)* = 0.30) and dashed red line (starburst extinction law from Calzetti et al. 1994 with an *E(B − V)* = 0.30). The filled black triangles mark ages of 2, 4, 6, 8, 10, 25, 50 and 100 Myr.

velocity = distance/age). As this object is one of the oldest ones (together with object 4) and also the closest one, it is similarly impossible for the other objects to have been thrown away from the disc of the main galaxy. This reasoning suggests that these young objects were formed in situ.

In Fig. 4 (top panel) we compared the FUV–NUV and FUV–*r* colours of the star-forming regions in NGC 2782 (black stars) with the regions detected in the tidal features of Arp 82 (green triangles) and Arp 305 (Hancock et al. 2007, 2009). We used these systems as a comparison sample, given that both systems present tidal tails with FUV, NUV and *R* (or *r*) photometry, which allow us to do a fair comparison with the photometric properties of the star-forming regions in NGC 2782. In the case of Arp 82, *R*-band magnitudes were converted into *r*-band magnitudes by using the transformation given in Lupton (2005) and the *g − r* colours of the 'bridge TDG' regions of Arp 305 (given that there are no *g − r* colours for regions in Arp 82). In the case of Arp 305, regions belonging to tidal features are marked with a blue circle, while objects detected in the 'bridge TDG' region are marked with red squares. In the bottom panel of Fig. 4 we compare the FUV–NUV colour versus the *r*-band absolute magnitude for the same regions. From both plots, we can see that regions in NGC 2782 have similar colours to those displayed by the star-forming regions in Arp 82 and Arp 305 (although they tend to cluster at the blue end of the FUV–*r* range), but being less luminous.

4.2 Main spectroscopic properties of the star-forming regions

In Fig. 5 (first three panels) we show the GMOS spectra (B600 grating) for the three regions located in the gaseous tidal tail of NGC 2782 for which spectroscopy was available. As expected from our selection criteria, these objects are very young. In the lowest panel of Fig. 5 we show the spectrum of the star-forming region located close to the main body of NGC 2782.

Figure 4. Top panel: *GALEX* FUV–NUV versus FUV–*r* of the star-forming regions in NGC 2782 (black stars), Arp 82 (green triangles) and Arp 305 (blue circles and red squares). Bottom panel: *r*-band absolute magnitude versus FUV–NUV colours. The symbols are the same as in the top panel. The data for Arp 82 and Arp 305 regions were taken from Hancock et al. (2007, 2009).

The three regions for which we have spectroscopy (5, 6 and 7) have radial velocities of 2556, 2531 and 2556 km s^{-1}, respectively, confirming that they are at the same distance as NGC 2782.

As described in Section 3.4 we corrected the blue part of the spectra of regions 5, 6 and 7 by Galactic extinction using a value of $E(B − V) = 0.08$. The results for the line ratios, all of them normalized to Hβ, are listed in Table 2.

Using the EW(Hβ) (single stellar population, Salpeter IMF and solar metallicity) we found ages of $\sim$4, $\sim$3 and $\sim$2 Myr for regions 5, 6 and 7, respectively. For regions 5 and 6, the spectroscopic estimate of the ages is in agreement with the age obtained from the colours, i.e. 2 and 3 Myr. In the case of region 7, the spectroscopic estimate of the age is lower than the age obtained from colours
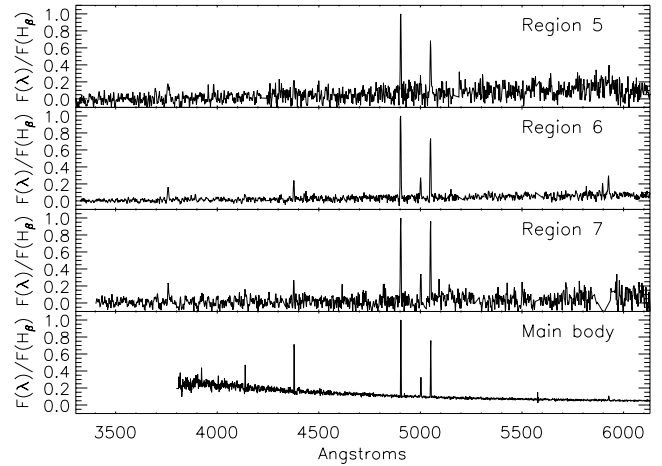
Figure 5. Gemini/GMOS B600 spectra of regions 5, 6 and 7 and SDSS spectrum for the compact source close to the disc of NGC 2782 (bottom spectrum). Spectra were normalized to the peak intensity at the Hβ line.

(6 Myr). These values are consistent within the uncertainties; however, we can not exclude an old stellar population co-existing with this star-forming region, similar to what was found in star-forming regions in the bridge of M81 and M82 (de Mello et al. 2008b).

Given that we are using semi-empirical and empirical calibrations in estimating the metallicities of the star-forming regions (and not direct estimates of these parameters), we adopt a fixed error of 0.2 dex in the case of the calibrations given by McGaugh (1991), as discussed in van Zee & Haynes (2006). We note that van Zee & Haynes (2006) found that oxygen abundances estimated by using the method shown in McGaugh (1991) could be overpredicted by 0.07 ± 0.10 dex. In the case of the calibrations given by Edmunds & Pagel (1984) we adopt an error of 0.31 dex, and in the case of Pilyugin (2001), we used an error of 0.2 dex, as suggested by the author.

For the region located close to the body of NGC 2782, with the SDSS spectrum, we found an oxygen abundance of $12+\log(O/H) = 8.72 \pm 0.10$ (using the N2 method, see Table 2). This value is closer to the upper branch of the R_{23} calibration curve than to the lower branch. In view of this fact, we speculate that abundances in regions 5, 6 and 7 can be estimated by using the upper branch of the R_{23} calibration. The oxygen abundances we derived for regions 5 and 7 (using Pilyugin 2001, Edmunds & Pagel 1984; McGaugh 1991, respectively) are listed in Table 2. The lowest oxygen abundance estimations were obtained by using the Pilyugin (2001) approach, while the highest values were obtained from the McGaugh (1991) method. Using this latter method, we found that regions 5, 6 and 7 have abundances of $12+\log(O/H) = 8.74 \pm 0.20$, 8.81 ± 0.20 and 8.78 ± 0.20, respectively, which are quite high values. It is interesting to note that if abundances in regions 5 and 6 were estimated by using the lower branch of the R_{23} calibration (see fig. 9 in McGaugh 1991), their abundances would be at most $12+\log(O/H)\sim7.8$, 7.7 and 7.8, respectively, and these results would have been quite different than the abundances estimated for the region located on the main disc of NGC 2782. By using the same data set, Werk et al. (2011) found abundances of $12+\log(O/H) = 8.66$, 8.72 and 8.56 for the same regions. Within the uncertainties, the abundances derived by us and by Werk et al. (2011) are consistent. In this case, our estimations of the oxygen abundances of the star-forming regions in NGC 2782 give an additional measure of the uncertainty on the metallicities of these systems.

Taking into account the uncertainties, sources 5, 6 and 7 have similar oxygen abundances to those derived for the nuclear region of NGC 2782, i.e. 12+log(O/H) = 8.63 (Moustakas & Kennicutt 2006, as estimated by using the recipe given in Pettini & Pagel 2004) and also are similar to the abundance determined by Engelbracht et al. (2008) for NGC 2782 (12+log(O/H) = 8.59 ± 0.10). By using the oxygen abundances of the regions listed above (plus two other objects), Werk et al. (2011) suggested a flat metallicity gradient for NGC 2782. Our analysis support this idea; however, new spectroscopic data for other H II regions along the western tidal tail of NGC 2782 are necessary to confirm this scenario.

The abundances of regions 5, 6 and 7 (listed in Table 2) are similar to the solar value given in Denicoló et al. (2002) and are higher (or of the same order) than the values found by Mendes de Oliveira et al. (2004), Duc & Mirabel (1998) and Croxall et al. (2009) for intergalactic H II regions and TDGs in interacting systems.

5 DISCUSSION

In this paper we have searched for star-forming regions in the gaseous tidal tail of the merger remnant NGC 2782. We used archival and new data to perform this analysis. Here, we summarize the main findings of our study.

(i) We have identified seven young UV-emitting sources in the H I tail of NGC 2782. Some of these regions are resolved in small clusters when high-resolution optical images are used.

(ii) All these objects have young ages (1 Myr < Age < 11 Myr) and masses ranging from $10^{3.9}$ to $10^{4.6}$ M$_\odot$.

(iii) Spectroscopic data for three of these objects confirm that they are at the same distance as NGC 2782. This result was also confirmed by Werk et al. (2011). We found that regions 5, 6 and 7 have high metallicities: 12+log(O/H) = 8.74, 8.81 and 8.78, respectively.

Some of the main issues concerning star formation outside galaxies are discussed below.

5.1 The physical parameters of the intergalactic star-forming regions in NGC 2782

In the past, a few authors have studied the properties of the stellar clusters in the gaseous tidal tail of NGC 2782. Using optical colours, Knierman (2007) found several blue clusters along the same tail. A few of our regions seem to be located at the same position as Knierman's clusters, as can be judged from their fig. 1 (they did not publish coordinates). Using Fabry–Perot observations, Bournaud et al. (2004) reported just one H II region in the H I tail of NGC 2782. We detect an object in the same location of Bournaud's H II region (region 6 in our work); however, we found several other similar objects in the H I tail. Probably the detection limit of the Fabry–Perot observations of Bournaud et al. could not reveal all the star-forming regions in the H I tail.

The fact that regions 5, 6 and 7 have quite high oxygen abundances suggests that these regions were formed from pre-enriched material. The material out of which these regions may have been formed could have been thrown out of the central region of the interacting galaxies that merged to form NGC 2782, forming the western gaseous tidal tail (scenario that is supported by *N*-body/smoothed particle hydrodynamics simulations, see Rupke, Kewley & Barnes 2010). If star formation events already took place in this tidal tail, these could have polluted the IGM with metals and with an underlying old stellar population. Bastian et al. (2009) found that young

stellar clusters can easily be destroyed within the first 10 Myr of their lives. Therefore, it remains plausible that the gaseous tidal tail of NGC 2782 already was a nursery of new stellar systems, which were destroyed by internal processes possibly through a phenomenon called *infant mortality* (see Section 5.3), polluting the medium with metals. This fact, plus the distance to the parent galaxy and the young ages that these object present, suggests that these star-forming systems were formed in situ.

We note that the three spectroscopically detected regions in this work have similar ages to the star-forming regions found by Mendes de Oliveira et al. (2004), by construction, given that we chose objects of similar colours. However, they are different of those objects since they have higher oxygen abundances. On the other hand, regions 5, 6 and 7 of this work have oxygen abundances comparable to the values displayed by the TDG candidates in the M81 system (Croxall et al. 2009).

5.2 Tidal tails: the birthplace of new stellar systems

Galaxy–galaxy interactions are an effective mechanism to strip neutral gas out of galaxy discs, forming extended gaseous tidal tails (e.g. Hibbard et al. 2001). Recently, Mullan et al. (2011) used the Wide Field Planetary Camera 2 on the *Hubble Space Telescope* to search for compact stellar structures in the tidal tails of a sample of 13 interacting galaxies, where NGC 2782 was included. These authors found an absence of cluster candidates in the western tidal tail of NGC 2782; however, by using *GALEX* and Gemini data we have catalogued several star-forming region candidates, with ages <11 Myr, in the gaseous western tidal tail of this system. All of our sources were detected in regions where the H I column densities reach values above the threshold to trigger star formation ($\log N_{HI}$ = 20.6 cm^{-2}) found by Maybhate et al. (2007) in their study of cluster formation in tidal debris.

In the western tidal tail of NGC 2782 no TDG was detected; however, several objects with IH II properties were found. Knierman et al. (2003) found a trend of formation of either TDGs or less massive systems but not both on tidal tails, for a sample of four mergers. In this context, the results found in this paper are in agreement with this previous work, given that NGC 2782 has only low-mass systems.

5.3 The fate of the star-forming regions in the H I tail of NGC 2782

Whether these systems will become independent entities is not clear. It will depend on several parameters, such as the distance to the parent galaxies and total masses. In this context, Mengel et al. (2008) compare the dynamical masses for nine young clusters in the Antennae (6–9 Myr) with respect to the photometric masses. They found that almost all clusters in the Antennae are stable and bound. Internal processes, as ionizing radiation coming from OB stars, stellar winds and supernova could remove the interstellar medium that binds young star-forming regions (as stellar clusters) and allow these objects to become gravitationally unbound systems, in a phenomenon called *infant mortality* (Fall, Chandar & Whitmore 2005). Recently, Bastian et al. (2009) found that infant mortality is more important in the first 10 Myr of a cluster, contrary to what was proposed by Whitmore, Chandar & Fall (2007), who found that the disruption of a cluster takes about 100 Myr. In this context, the continuous formation of stellar clusters along the time, which are subsequently disrupted by the *infant mortality* process, could increase the metallicity of a given region just due to stellar evolution.

In the case of NGC 2782, the high oxygen abundance present at large distances from the main body of the system suggests that the IGM is already rich in metals. If the *infant mortality* process already took place in this system, it could explain, at some level, the high metallicity observed in the gaseous tidal tail of NGC 2782.

5.4 Where is the molecular gas in merger galaxies?

Although there is a good correlation between the location of UV sources with the presence of peaks in the H I distribution in tidal tails (e.g. Neff et al. 2005; de Mello et al. 2008a), it is well known that stars form in molecular clouds. As Knierman (2007) noted for NGC 2782, it is an unexpected result to find star formation in regions without molecular gas. Our analysis shows that several UV sources are located in the same region of the blue clusters of Knierman, where H I has been detected. In view of this scenario, where is the molecular gas in merger systems? Using a sample of seven mergers, Bryant & Scoville (1999) found that the molecular gas is concentrated in the core of the mergers. In a similar way, Yun & Hibbard (2001) found that the CO emission in mergers is placed in the central 2 kpc radius. Studying a sample of TDGs, Braine et al. (2001) detected CO in six objects of their sample. Smith (1991) found an H I mass of 1.4×10^9 M$_\odot$ in the north-east tail of NGC 2782. Interestingly, neither Smith et al. (1999) nor Braine et al. (2001) could detect CO in the location of the UV-emitting regions in NGC 2782.

Therefore, the results shown in this paper imply that star formation took place in the tidal tail a few million years ago. The lack of CO detection can be explained if we take into account Heithausen & Walter (2000) results using the same instrument (and beam size) as Braine et al. (2001). They detected two molecular complexes in the nearby galaxy NGC 3077. Complex 2 has a molecular mass of $M = 4 \times 10^6$ M$_\odot$. This mass and their respective CO flux at the distance of NGC 2782 ($S = 0.32$ Jy km s^{-1}, using equation 4 of Braine et al. 2001) are below the values that Braine et al. (2001) defined as *no detection of molecular gas* for NGC 2782 ($S \leq 0.5$ Jy km s^{-1}). In a similar way, Walter, Martin & Ott (2006) studied the molecular gas in the tidal arms near to NGC 3077 using interferometric data. They found several H II regions over the H I distribution in this area and one of these regions (object A) is associated with a molecular cloud complex. If we take the flux of this region ($S = 8.2$ Jy km s^{-1}), located at 3.6 Mpc, and carry it to the distance of the stellar clusters found in NGC 2782, this region has a flux of $S = 0.09$ Jy km s^{-1} and it could not be detected in CO, following table 2 in Braine et al. (2001). Our detected regions seem to be small objects, with typical masses of stellar clusters; therefore, their masses of molecular gas could be low enough to remain undetected by present observations at the distances of our targets.

6 CONCLUSIONS

In this paper we found seven young UV-emitting sources in the gaseous tidal tail of the system NGC 2782. All these regions have stellar masses and ages typical of IH II. They are located across the H I distribution and not specifically on H I peaks, as also was reported by Mendes de Oliveira et al. (2004) for the IH II in the Stephan's Quintet and by Walter et al. (2006) for NGC 3077. When an optical *r*-band image is taken into account, these UV sources can be resolved in several smaller systems. We found that three objects (regions 5, 6 and 7) have high metallicities (12+log(O/H) = 8.74 ± 0.20, 8.81 ± 0.20 and 8.78 ± 0.20, respectively). This result could be explained if some high-abundance gas from the

centre of the merging galaxies could be expelled, forming tidal tails. An additional contribution for the observed high abundances could be related to star formation events. In this case, the process known as *infant mortality*, which predicts that stellar clusters are dissolved after ~10 Myr, could help explaining the observed high metallicities. Further spectroscopic data are necessary to constrain the membership of other detected regions in the vicinity of the interacting system, to study metallicities, to know how the IGM is enriched by this type of object and to compare dynamical and photometric masses, in order to know the fate of these systems.

REFERENCES

Abazajian et al., 2009, ApJS, 182, 543
Amôres E. B., Lépine J. R. D., 2005, AJ, 130, 659
Bastian N., Trancho G., Konstantopoulos I. S., Miller B. W., 2009, ApJ, 701, 607
Bertin E., Arnouts S., 1996, A&AS, 117, 393
Bohlin R. C., Savage B. D., Drake J. F., 1978, ApJ, 224, 132
Boquien M. et al., 2009, AJ, 137, 4561
Boquien M., Duc P.-A., Galliano F., Braine J., Lisenfeld U., Charmandaris V., Appleton P. N., 2010, AJ, 140, 2124
Bournaud F., Duc P. A., Amram P., Combes F., Gach J.-L., 2004, A&A, 425, 813
Braine J., Duc P.-A., Lisenfeld U., Charmandaris V., Vallejo O., Leon S., Brinks E., 2001, A&A, 378, 51
Brocklehurst M., 1971, MNRAS, 153, 471
Bryant P. M., Scoville N. Z., 1999, AJ, 117, 2632
Calzetti D., Kinney A. L., Storchi-Bergmann T., 1994, ApJ, 429, 582
Cardelli J. A., Clayton G. C., Mathis J. S., 1989, ApJ, 345, 245
Cerviño M., Valls-Gabaud D., 2003, MNRAS, 338, 481
Cerviño M., Luridiana V., Pérez E., Vílchez J. M., Valls-Gabaud D., 2003, A&A, 407, 177
Croxall K. V., van Zee L., Lee H., Skillman E. D., Lee J. C., Côté S., Kennicutt R. C., Miller B. W., 2009, ApJ, 705, 723
da Silva R. L., Fumagalli M., Krumholz M., 2012, ApJ, 745, 145

de Mello D. F., Torres-Flores S., Mendes de Oliveira C., 2008a, AJ, 135, 319

de Mello D. F., Smith L. J., Sabbi E., Gallagher J. S., Mountain M., Harbeck D. R., 2008b, AJ, 135, 548

de Mello D. F., Urrutia-Viscarra F., Mendes de Oliveira C., Torres-Flores S., Carrasco E. R., Cypriano E., 2012, MNRAS, submitted

Denicoló G., Terlevich R., Terlevich E., 2002, MNRAS, 330, 69

Dopita M. A., Evans I. N., 1986, ApJ, 307, 431

Duc P.-A., Mirabel I. F., 1998, A&A, 333, 813

Edmunds M. G., Pagel B. E. J., 1984, MNRAS, 211, 507

Engelbracht C. W., Rieke G. H., Gordon K. D., Smith J.-D. T., Werner M. W., Moustakas J., Willmer C. N. A., Vanzi L., 2008, ApJ, 678, 804

Fall S. M., Chandar R., Whitmore B. C., 2005, ApJ, 631, L133

Fitzpatrick E. L., 1999, PASP, 111, 63

Hancock M., Smith B. J., Struck C., Giroux M. L., Appleton P. N., Charmandaris V., Reach W. T., 2007, AJ, 133, 79

Hancock M., Smith B. J., Giroux M. L., Struck C., 2008, MNRAS, 389, 1470

Hancock M., Smith B. J., Struck C., Giroux M. L., Hurlock S., 2009, AJ, 137, 4643

Heithausen A., Walter F., 2000, A&A, 361, 500

Hibbard J. E., van Gorkom J. H., Rupen M. P., Schiminovich D., 2001, in Hibbard J. E., Rupen M. P., van Gorkom J. H., eds, ASP Conf. Ser. Vol. 240, Gas and Galaxy Evolution. Astron. Soc. Pac., San Francisco, p. 657

Hodge P. W., Kennicutt R. C., 1983, AJ, 88, 296

Hunt L. K. et al., 2008, A&A, 482, 133

Jogee S., Kenney J. D. P., Smith B. J., 1998, ApJ, 494, L185

Knierman K., 2007, Island Universes, Astrophysics and Space Science Proceedings. Springer, 2007, p. 307

Knierman K. A., Gallagher S. C., Charlton J. C., Hunsberger S. D., Whitmore B., Kundu A., Hibbard J. E., Zaritsky D., 2003, AJ, 126, 1227

Leitherer C. et al., 1999, ApJS, 123, 3

Lupton R. 2005, SDSS website (http://www.sdss.org/dr5/algorithms/sdssUBVRITransform.html#Lupton2005)

McCall M. L., Rybski P. M., Shields G. A., 1985, ApJS, 57, 1

McGaugh S. S., 1991, ApJ, 380, 140

Martin D. C. et al., 2005, ApJ, 619, L1

Maybhate A., Masiero J., Hibbard J. E., Charlton J. C., Palma C., Knierman K. A., English J., 2007, MNRAS, 381, 59

Mendes de Oliveira C., Cypriano E. S., Sodré L., Jr, Balkowski C., 2004, ApJ, 605, L17

Mendes de Oliveira C., Temporin S., Cypriano E. S., Plana H., Amram P., Sodré L., Jr, Balkowski C., 2006, AJ, 132, 570

Mengel S., Lehnert M. D., Thatte N. A., Vacca W. D., Whitmore B., Chandar R., 2008, A&A, 489, 1091

Minchin R. F. et al., 2003, MNRAS, 346, 787

Mirabel I. F., Dottori H., Lutz D., 1992, A&A, 256, L19

Morrissey P. et al., 2005, ApJ, 619, L7

Moustakas J., Kennicutt R. C., Jr, 2006, ApJS, 164, 81

Mullan B. et al., 2011, ApJ, 731, 93

Mundell C. G., James P. A., Loiseau N., Schinnerer E., Forbes D. A., 2004, ApJ, 614, 648

Neff S. G. et al., 2005, ApJ, 619, L91

Pettini M., Pagel B. E. J., 2004, MNRAS, 348, L59

Pilyugin L. S., 2001, A&A, 369, 594

Popescu B., Hanson M. M., 2010, ApJ, 724, 296

Rupke D. S. N., Kewley L. J., Barnes J. E., 2010, ApJ, 710, L156

Savage B. D., Mathis J. S., 1979, ARA&A, 17, 73

Schelegel D. J., Finkbeiner D. P., Davis M., 1998, ApJ, 500, 525

Schweizer F., 1980, ApJ, 237, 303

Schweizer F., 1982, ApJ, 252, 455

Seibert M. et al., 2005, ApJ, 619, L55

Smith B. J., 1991, ApJ, 378, 39

Smith B. J., 1994, AJ, 107, 1695

Smith B. J., Struck C., Kenney J. D. P., Jogee S., 1999, AJ, 117, 1237

Smith B. J. et al., 2008, AJ, 135, 2406

Smith B. J., Giroux M. L., Struck C., Hancock M., 2010, AJ, 139, 1212

Thilker D. A. et al., 2007, ApJS, 173, 538

Torres-Flores S., Mendes de Oliveira C., de Mello D. F., Amram P., Plana H., Epinat B., Iglesias-Páramo J., 2009, A&A, 507, 723

Torres-Peimbert S., Peimbert M., Fierro J., 1989, ApJ, 345, 186

Tran H. D. et al., 2003, ApJ, 585, 750

van Zee L., Haynes M. P., 2006, ApJ, 636, 214

Walter F., Martin C. L., Ott J., 2006, AJ, 132, 2289

Weilbacher P. M., Duc P.-A., Fritze-v. Alvensleben U., Martin P., Fricke K. J., 2000, A&A, 358, 819

Weilbacher P. M., Duc P.-A., Fritze-v. Alvensleben U., 2003, A&A, 397, 545

Werk J. K., Putman M. E., Meurer G. R., Santiago-Figueroa N., 2011, ApJ, 735, 71

Whitmore B. C., Chandar R., Fall S. M., 2007, AJ, 133, 1067

Yoshida M., Taniguchi Y., Murayama T., 1994, PASJ, 46, 195

Yun M. S., Hibbard J. E., 2001, ApJ, 550, 104

This paper has been typeset from a TEX/LATEX file prepared by the author.